Journal of AppliedMath 2024, 2(6), 2209.
https://doi.org/10.59400/jam2209

Article

Multistability and organization of chaos and quasiperiodicity in a memristor-based Shimizu-Morioka oscillator under two-frequency excitation

Paulo Cesar Rech

Departamento de Física, Universidade do Estado de Santa Catarina, 89219-710 Joinville, Brazil; paulo.rech@udesc.br

CITATION

Rech PC. Multistability and organization of chaos and quasiperiodicity in a memristor-based Shimizu-Morioka oscillator under two-frequency excitation. Journal of AppliedMath. 2024; 2(6): 2209. https://doi.org/10.59400/jam2209

ARTICLE INFO

Received: 4 December 2024
Accepted: 27 December 2024
Available online: 30 December 2024

COPYRIGHT

Copyright © 2024 Author(s). *Journal of AppliedMath* is published by Academic Publishing Pte. Ltd. This work is licensed under the Creative Commons Attribution (CC BY) license. https://creativecommons.org/licenses/by/4.0/

Abstract: In this paper we investigate the organization of chaos and quasiperiodicity in a parameter plane of a continuous-time three-dimensional nonautonomous dynamical system. More specifically, we investigate a memristor-based Shimizu-Morioka oscillator, where the external excitation is represented by the sum of two different sinusoidal functions with angular frequencies ω_1 and ω_2. Through a scan carried out in the (ω_1, ω_2) parameter plane, with the dynamical behavior of each point in the phase-space being characterized by the Lyapunov exponents spectrum, we show that this system presents chaos and quasiperiodicity regions, without presenting, however, periodicity regions. Parameter regions for which the multistability phenomenon was detected, also are observed. Basins of attraction of coexisting chaotic and quasiperiodic attractors, as well as the attractors themselves, are reported.

Keywords: Shimizu-Morioka oscillator; parameter plane; Lyapunov exponents; multistability
PACS Classification:: 05.45.-a; 05.45.Tp; 05.10.-a

1. Introduction

In this paper we report on a three-dimensional nonautonomous dynamical system, namely the so-called memristor-based Shimizu-Morioka oscillator [1–5], which is modeled by a nonautonomous nonlinear set of three first-order ordinary differential equations. Such a system was proposed by Durairaj and co-workers [4], being mathematically expressed by

$$\begin{aligned} \dot{x} &= y \\ \dot{y} &= x - ay - xz + bM(x)y + f_1 \sin(\omega_1 t) + f_2 \sin(\omega_2 t) \\ \dot{z} &= -dz + x^2 \end{aligned} \tag{1}$$

where x, y, z are the state dynamical variables, and a, b, d are the control parameters of the *original* Shimizu-Morioka oscillator [1–5]. The function $M(x) = c + x^2$ represents the memristive function, with c being an additional parameter, and f_1 (f_2), ω_1 (ω_2) are, respectively, the amplitude and the angular frequency of the external sinusoidal forcing 1 (2). Durairaj et al. [4] reports on strange nonchaotic attractors [6] detected in the phase-space of the two-frequency forced memristor-based Shimizu-Morioka oscillator modeled by system Equation (1). The entire investigation carried out by the authors considers the variation of just one of the frequencies of the external forcing, namely ω_1, keeping the other parameters constant.

The contribution reported in our article aims to advance knowledge about system Equation (1), starting with the generation of the three (ω_1, ω_2) parameter

plane panels shown in **Figure 1**, therefore considering the simultaneous variation of both external angular frequencies. Note that all the panels in **Figure 1** consider the same range of parameters, and what differentiates them is the initial condition used in the numerical integration process of the system of differential Equation (1). This numerical integration is a mandatory procedure, to generate the time series necessary to compute the Lyapunov exponents spectrum which characterize the dynamical behavior of each point in the (ω_1, ω_2) parameter plane. As we will see in detail in the next two sections, the panels in **Figure 1**, together with others showing enlargements of suitable regions of these same panels, will allow us to observe regions where the phenomenon known as multistability [7] occurs. They will also allow us to observe regions where quasiperiodic structures embedded in a chaotic region, appear organized. Ultimately, such panels will allow us to contemplate the entire organization of chaos and quasiperiodicity in the (ω_1, ω_2) parameter plane of system Equation (1).

The rest of this report is organized as follows. Section 2 is devoted to present results of a numerical investigation concerning the occurrence of multistability in system Equation (1), while Section 3 is dedicated to results related to the organization of chaos and quasiperiodicity in the (ω_1, ω_2) parameter plane. The report is summarized in Section 4.

2. Multistability

Each of the panels in **Figure 1** shows the same global view of the (ω_1, ω_2) parameter plane of system Equation (1), for $0 \leq \omega_1, \omega_2 \leq 6$, and other parameters kept fixed as $a = 0.8$, $b = 0.22$, $c = -2$, $d = 0.4$, $f_1 = 0.5$, $f_2 = 0.4$. The dynamical behavior of each point is characterized by the magnitude of the largest Lyapunov exponent (LLE), to which a color is associated according to the color bar to the right of each panel. Parameter regions with a positive LLE are painted in a color that ranges from yellow to red, and are related to chaotic attractors in the phase-space. Parameter regions painted in black in turn are related to regular (periodic or quasiperiodic) attractors in the phase-space, and have LLE= 0.

As we will see below, each panel in **Figure 1** was generated in a different way, but they all use the LLE, computed by using a home-made FORTRAN code based in the algorithm in Wolf and collaborators [8] to characterize the dynamical behavior for each choice of ω_1 and ω_2 in the respective parameter plane panel. Regardless of the panel under consideration, the parameter ranges were discretized in a mesh of $10^3 \times 10^3$ points, with system Equation (1) being numerically integrated by using the fourth-order Runge-Kutta algorithm, with a time step equal to 10^{-3}. The average involved in the computation of each of the 10^6 LLEs takes into account 4×10^6 integration steps, after discarding a transient behavior of 2×10^6 integration steps.

The panel in **Figure 1a** was generated always from a same arbitrarily chosen initial condition $(x_0, y_0, z_0) = (0.1, 0.2, 0.3)$, regardless of the values of the parameters ω_1 and ω_2. Once the values of ω_1 and ω_2 have been defined, system Equation (1) is numerically integrated with consequent obtaining of the respective time series, and the Lyapunov exponents spectrum is computed. In order to generate the panel in **Figure 1b**, we fix $(\omega_1, \omega_2) = (0, 0)$, and initialize system Equation (1) with an

arbitrary initial condition $(x_0, y_0, z_0) = (0.1, 0.2, 0.3)$. Then system Equation (1) is numerically integrated, the respective time series obtained, and the related Lyapunov exponents spectrum is computed. Parameter ω_1 is increased, and system Equation (1) is initialized with the variables related to the final point obtained for the prior value of ω_1. The numerical integration is performed, and a new Lyapunov exponents spectrum is computed from the new time series obtained. The procedure reported in the previous sentence is repeated until ω_1 reaches its largest value, namely 6. Then parameter ω_2 is increased, and the entire procedure is repeated until the parameter set $(\omega_1, \omega_2) = (6, 6)$ is considered in computing. The panel in **Figure 1c** in turn is generated in a manner analogous to that in **Figure 1b**, but starting in $(\omega_1, \omega_2) = (6, 6)$ and ending in $(\omega_1, \omega_2) = (0, 0)$. In short, the panel in **Figure 1b**,**c** was generated by using the method *following the attractor* along lines of constant ω_2, increasing (decreasing) ω_1 from 0 (6) to 6 (0).

Looking less closely at the panels in **Figure 1**, they do not seem to present any differences. Taking a closer look, however, allows us to notice significant differences, particularly in the region inside the two narrowest boxes. As regards either of these two narrowest boxes, the region inside each of them appears painted differently in each of the panels. Regions that appear black in one of the panels eventually appear yellow in another panel and vice versa, meaning that the dynamical behavior changes from regular to chaotic, or from chaotic to regular. If we choose a specific point in the parameter plane where such behavior occurs, we will have that the set of parameters of the system Equation (1) will be completely fixed, but the dynamical behavior may be different, namely regular or chaotic, depending on the way the parameter plane itself is generated. Therefore, we have just identified two regions in the (ω_1, ω_2) parameter plane, inside each of the two narrowest boxes, whose long-term dynamical behavior can be different, depending on the initial condition adopted for the numerical integration of system Equation (1). We can then ensure that system Equation (1) presents at least more than one coexisting attractors in their phase-space, for a kept fixed set of parameters (ω_1, ω_2) in some points of these regions, and this is a signature of the multistability phenomenon [7].

What makes multistable systems worth of study is their importance from both a theoretical and a technological point of view. Multistable systems have been investigated in the most varied fields of knowledge since a long time ago [9–13], until more recent times [14–23]. Some examples of systems where multistability is present include ring cavity lasers [9], semiconductor lattices [12], fluid dynamics [13], electronic circuits [14,17], biology [15,18,20,21], and plasma physics [22,23].

In order to shed more light on the investigation of multistability in system Equation (1), we generate the bifurcation diagrams shown in **Figure 2**, all of them using the scheme *following the attractor*. In each of them are shown the local maxima (the peaks) of the variable x, denoted by x_m, in one complete trajectory in the phase-space, for one thousand values of the respective parameter (ω_1 or ω_2).

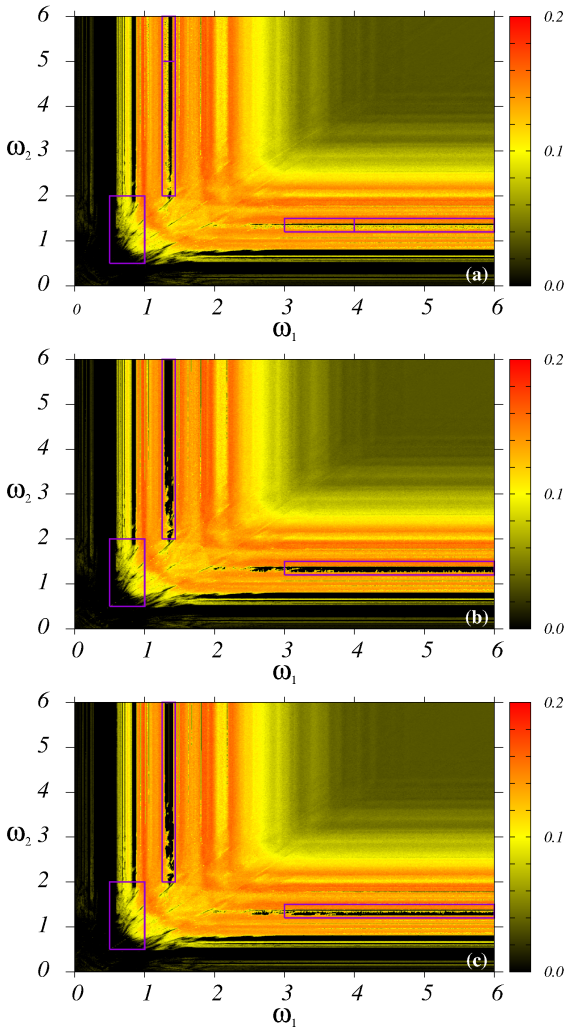

Figure 1. Shown are three (ω_1, ω_2) parameter plane plots for system Equation (1), relating different color intensities to different magnitudes of the largest Lyapunov exponent, as the scale shown in the column at right side of each panel, (**a**) same initial condition, regardless of the values of ω_1 and ω_2; (**b**) following the attractor from $(\omega_1, \omega_2) = (0, 0)$ to $(\omega_1, \omega_2) = (6, 6)$; (**c**) following the attractor from $(\omega_1, \omega_2) = (6, 6)$ to $(\omega_1, \omega_2) = (0, 0)$.

The two bifurcation diagrams in **Figure 2a** were constructed for points on the line segment $\omega_2 = 5.0$, between $\omega_1 = 1.27$ and $\omega_1 = 1.42$, drawn in the region of the left box in **Figure 1a**. The bifurcation diagram represented by black points considers the increase of the parameter ω_1 from 1.27 to 1.42, while that represented by red points considers the decrease of ω_1 from 1.42 to 1.27. It is clear that the bifurcation diagram in black is different from the one in red, since black points do not coincide with red points throughout the entire length of **Figure 2a**. It is exactly this difference between the two bifurcation diagrams that indicates the presence of the multistability phenomenon in the system under study. In the region on the left, for $1.27 \leq \omega_2 \leq 1.28$, we have a region where two chaotic attractors are coexisting, since both the black and red points are scattered in the region, but are not coincident. In the region on the right, for $1.402 \leq \omega_2 \leq 1.42$, we have a region where a chaotic attractor (points in red, LLE > 0) coexists with a quasiperiodic attractor (points in black, LLE = 0 and second LLE = 0). In the region between these two regions, for $1.28 \leq \omega_2 \leq 1.402$, the coexistence is of two

quasiperiodic attractors.

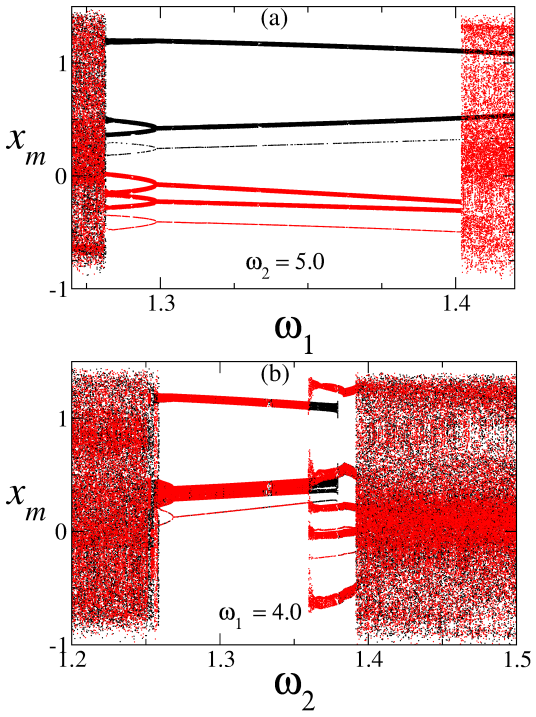

Figure 2. (**a**) Two bifurcation diagrams for points along the line segment $\omega_2 = 5.0$, between $\omega_1 = 1.27$ and $\omega_1 = 1.42$ in **Figure 1a**,**b** two bifurcation diagrams for points along the line segment $\omega_1 = 4.0$, between $\omega_2 = 1.2$ and $\omega_1 = 1.5$ in **Figure 1b**. Regardless of the panel, bifurcation diagrams in black (red) consider the increase (decrease) of the respective parameter.

The two bifurcation diagrams in **Figure 2b**, in turn, were constructed for points on the line segment $\omega_1 = 4.0$, between $\omega_2 = 1.2$ and $\omega_2 = 1.5$, drawn in the region of the right box in **Figure 1a**. As before, the bifurcation diagram in black considers the increase of the parameter, this time ω_2, from 1.2 to 1.5, while the one in red considers the decrease of ω_2 from 1.5 to 1.2. Again it is clear that the bifurcation diagram in black is different from the one in red, and again we detect the presence of the multistability phenomenon in the system under study. In the left and right regions, respectively for $1.2 \leq \omega_2 \leq 1.259$ and $1.393 \leq \omega_2 \leq 1.5$, there are coexistence of two chaotic attractors. Multistability also is present, this time with the coexistence of two quasiperiodic attractors in a small region between these two regions, namely the one for which $1.36 \leq \omega_2 \leq 1.393$.

As an example, **Figure 3a** shows basins of attraction of chaotic attractors, in red, and of quasiperiodic attractors, in black. Actually, **Figure 3a** shows a (x_0, y_0) initial conditions cross-section of three-dimensional (x_0, y_0, z_0) basins of attraction for system Equation (1), namely the one for which $z_0 = 1.0$, and $(\omega_1, \omega_2) = (1.41, 5.0)$, a point located on the small line segment $\omega_2 = 5.0$ drawn in **Figure 1a**, a point also easily located at right in **Figure 2a**. As we can see in **Figure 3a**, the vast majority of initial condition points belong to the basin of attraction of the chaotic attractor (red region). The basins of attraction of the quasiperiodic attractor in turn are made up of a set of eight small disconnected regions, with well-defined boundaries. This means that the points belonging to the chaotic basin are perfectly distinguishable from the points belonging

to the quasiperiodic basin. In summary, basins of attraction in **Figure 3a** indicate with good precision, initial condition points leading to either of the two attractors in the phase-space, chaotic or quasiperiodic. Accordingly, since the parameters in system (1) are kept fixed at $(\omega_1, \omega_2) = (1.41, 5.0)$, $a = 0.8$, $b = 0.22$, $c = -2$, $d = 0.4$, $f_1 = 0.5$, $f_2 = 0.4$, and for $z_0 = 1.0$, an initial condition point (x_0, y_0) chosen in the red region takes the system to a chaotic attractor in the phase-space, whereas an initial condition point (x_0, y_0) chosen in the black region takes the system to a quasiperiodic attractor.

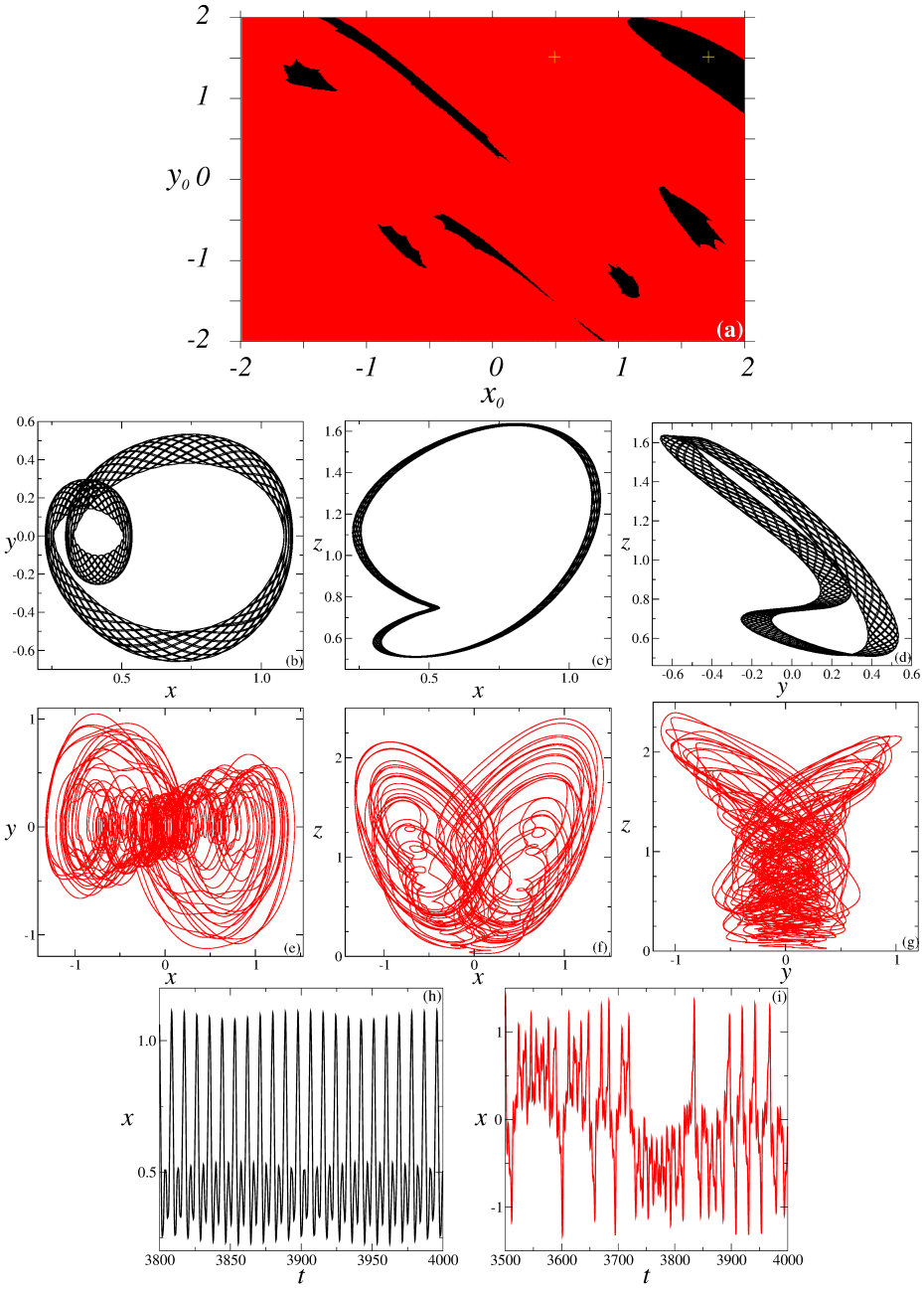

Figure 3. (**a**) Projection of basins of attraction for system Equation (1) on the (x_0, y_0) initial conditions plane, for $z_0 = 1.0$. Black (Red) is related to a quasiperiodic (chaotic) attractor basin. In (**b**,**c**,**d**) and (**e**,**f**,**g**) are shown, respectively, two-dimensional projections of the coexisting quasiperiodic and chaotic attractors. (**h**) and (**i**) show the temporal evolution of the variable x for the coexisting quasiperiodic and chaotic attractors.

To illustrate, **Figure 3** also shows all two-dimensional projections of two coexisting attractors, namely a quasiperiodic one in the middle row, and a chaotic one in the bottom row, all of them generated for $(\omega_1, \omega_2) = (1.41, 5.0)$, $a = 0.8$, $b = 0.22$, $c = -2$, $d = 0.4$, $f_1 = 0.5$, and $f_2 = 0.4$. Therefore, **Figure 3b**,**d** show two-dimensional projections of a quasiperiodic attractor, and **Figure 3e**,**g** show two-dimensional projections of a chaotic attractor. For the quasiperiodic attractor the initial condition is $(x_0, y_0, z_0) = (1.7, 1.5, 1.0)$, corresponding to the point marked with a plus sign in one of the black region in **Figure 3a**, while for the chaotic attractor the initial condition is $(x_0, y_0, z_0) = (0.5, 1.5, 1.0)$, corresponding to the point also marked with a plus sign, but this time in the red region of the same **Figure 3a**. Also to illustrate, diagrams in **Figure 3h,i** show the time series for the variable x, for the coexisting quasiperiodic and chaotic attractors.

3. Chaos and quasiperiodicity

Figure 4a shows a magnification of the region inside the box on the bottom left in panels of **Figure 1**, where we can see, in the region inside the box drawn on it, regular structures embedded in a parameter region for which the system exhibits chaotic behavior. To be more specific, such structures are related to parameters for which the behavior of the system in phase-space is quasiperiodic, since in addition to the largest LLE, the second LLE is also null as we will show later. The existence of these quasiperiodic regions in the (ω_1, ω_2) parameter plane is justified by the existence of two excitation mechanisms in system Equation (1), namely the two sinusoidal functions with different angular frequencies. There are apparently an infinite number of sets of these quasiperiodic structures, three of them being highlighted, each by a line segment in **Figure 4b** which in turn displays the magnification of the region inside the box in **Figure 4a**, and will best serve to obtain the results that follow.

Each panel in **Figure 5** shows bifurcation diagrams, in green, and plots of the LLE and the second LLE, respectively in blue and red. Bifurcation diagrams were generated in a similar way to those shown in **Figure 2**, displaying, therefore, the local maxima of the variable x (x_m), for one thousand values of ω_1. Bifurcation diagram in **Figure 5a** is related to points along the line segment $\omega_2 = -1.33\omega_1 + 2.44$ crossing the quasiperiodic structures above in **Figure 4b**. The one shown in **Figure 5b** is related to points along the line segment $\omega_2 = -0.5\omega_1 + 1.85$ crossing the middle quasiperiodic structures in **Figure 4b**, while the one shown in**Figure 5c** in turn is related to points along the line segment $\omega_2 = -13\omega_1 + 9.28$ crossing the quasiperiodic structures below in **Figure 4**. LLE and second LLE were also computed for points along the line segments given above, so in each panel of **Figure 5** the bifurcation diagrams and the Lyapunov exponent graphs are directly related.

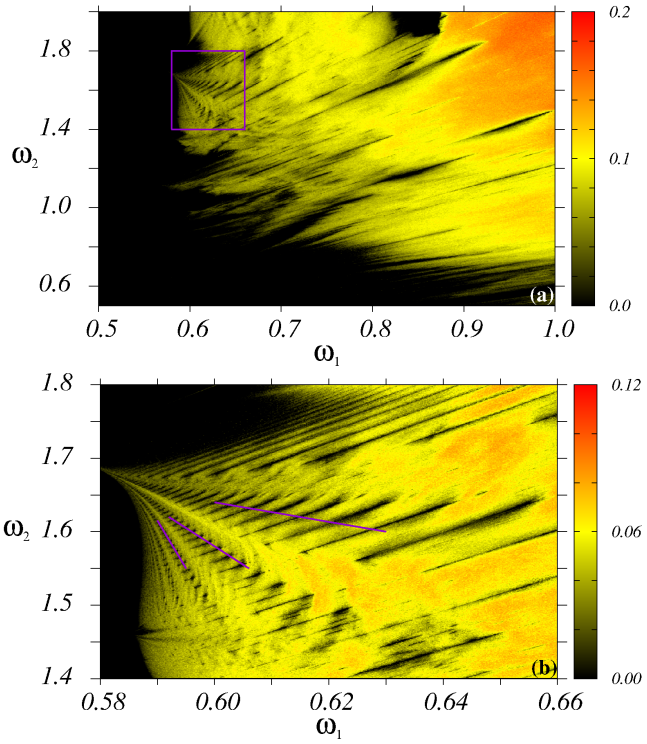

Figure 4. (**a**) Magnification of the region inside the box on the bottom left in panels of **Figure 1**. In (**b**) is shown a magnification of the region inside the box in (**a**).

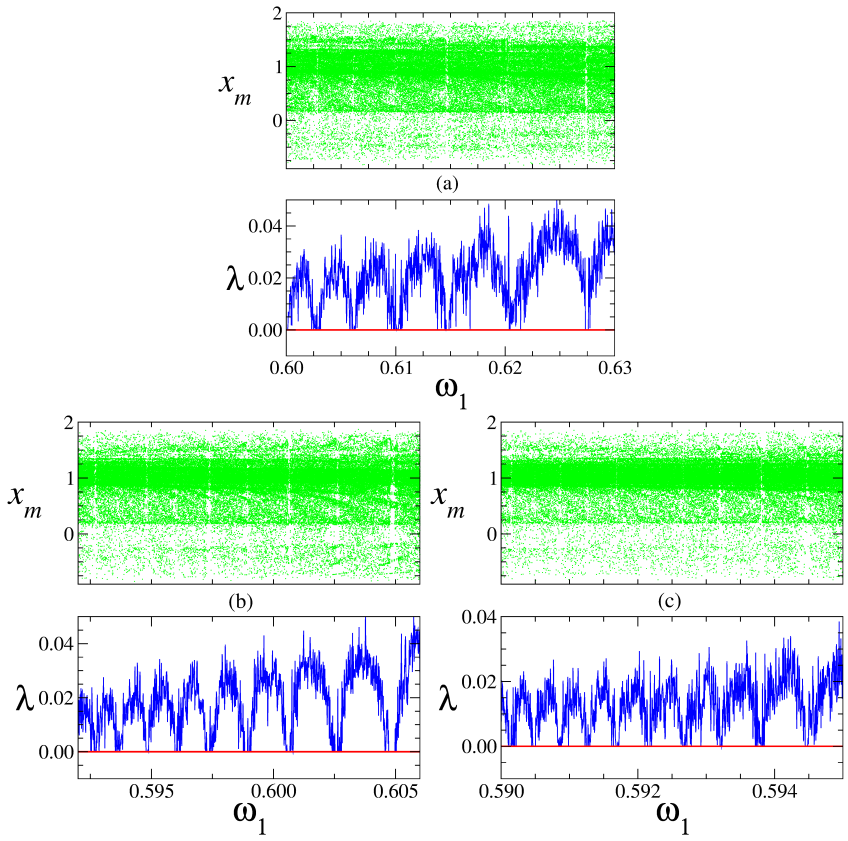

Figure 5. (**a**) Shown are bifurcation diagram and related plots of the LLE and the second LLE, for points along the top straight line in **Figure 4b**; (**b**) same graphs as in (**a**), for points along the middle straight line in **Figure 4b**; (**c**) same graphs as in (**a**) and (**b**) for points along the straight line below in **Figure 4b**.

Regardless of the panel considered in **Figure 5**, we observe that the second LLE is always null, while the LLE itself is greater than or equal to zero throughout the range of ω_1 considered. We also observe that the bifurcation diagrams show an extensive region of parameters ω_1 for which the system operates in a chaotic regime, which is characterized by a LLE greater than zero, with a corresponding second LLE equal to zero. There are, however, embedded in this chaotic region several quasiperiodicity windows, some not so visible in the bifurcation diagrams of **Figure 5**, characterized by both LLE and the second LLE equal to zero. These are regions for which the system operates in a quasiperiodic regime. In the entire range of (ω_1, ω_2) considered in our study, no regions of parameters related to periodic behavior in phase-space, for which only the LLE is equal to zero, were observed.

4. Summary

In this paper we report on the organization of chaos and quasiperiodicity in a parameter plane of a continuous-time three-dimensional nonautonomous dynamical system, namely the system that models a memristor-based Shimizu-Morioka oscillator, where the external forcing is represented by the sum of two sinusoidal functions with different angular frequencies ω_1 and ω_2. We have used Lyapunov exponents spectra to characterize the dynamics in points of the (ω_1,ω_2) parameter plane. We have shown that the investigated system presents only chaos and quasiperiodicity regions in the aforementioned parameter plane. We also have observed parameter regions for which the multistability phenomenon is perfectly characterized, a fact that is proven by graphs of basins of attraction of coexisting chaotic and quasiperiodic attractors, and graphs of the attractors themselves.

Acknowledgments: The author thanks Conselho Nacional de Desenvolvimento Científico e Tecnológico-CNPq, and Fundação de Amparo à Pesquisa e Inovação do Estado de Santa Catarina-FAPESC, Brazilian Agencies, for financial support.

Data availability: The data that support the findings of this investigation are available from the corresponding author upon reasonable request.

Conflict of interest: The author declares no conflict of interest.

References

1. Shimizu T, Morioka N. On the bifurcaion of a symmetric limit cicle to an asymmetric one in a simple model. Phys. Lett A. 1980; 76(3–4): 201–204.
2. Wen Z, Li Z, Li X. Bursting oscillations and bifurcation mechanism in memristor-based Shimizu-Morioka system with two time scales. Chaos, Solitons Fractals. 2019; 128: 58–70.
3. Huang K, Shi S, Li W. Integrability analysis of the Shimizu-Morioka system. Commun. Nonlinear Sci. Numer. Simulat. 2020; 84: 105101.
4. Durairaj P, Kanagaraj S, Kathamuthu T, Rajagopal K. Strange nonchaotic attractors in memristor-based Shimizu-Morioka oscillator. Int. J. Bifurcat. Chaos. 2022; 32: 2230022.
5. Thamilmaran K, Thamilvizhi T, Kuramasamy S, Durairaj P. Experimental observation of extreme events in the Shimizu-Morioka oscillator. Int. J. Bifurcat. Chaos. 2023; 33: 2330039.
6. Grebogi C, Ott E, Pelikan S, Yorke JA. Strange attractors that are not chaotic. Physica. D. 1984; 13(1–2): 261–268.

7. Feudel U, Grebogi C. Multistability and the control of complexity. Chaos. 1997; 7(4): 597–604.
8. Wolf A, Swift JB, Swinney HL, Vastano JA. Determining Lyapunov exponents from a time series. Physica. D. 1985; 6(3): 285–317.
9. Hammel SM, Jones CKRT, Moloney JV. Global dynamical behavior of the optical field in a ring cavity. J. Opt. Soc. Am. B. 1985; 2: 552.
10. Marmillot P, Kaufman M, Hervagault J. Multiple steady states and dissipative structures in a circular and linear array of three cells: Numerical and experimental approaches. J. Chem. Phys. 1991; 95: 1206–1214.
11. Schiff SJ, Jerger K, Duong DH, et al. Controlling chaos in the brain. Nature. 1994; 370: 615–620.
12. Prengel F, Wacker A, Schöll E. Simple model for multistability and domain formation in semiconductor superlattices. Phys. Rev. B. 1994; 50: 1705.
13. Yoden S. Classification of simple low-order models in geophysical fluid dynamics and climate dynamics. Nonlinear Anal. Theory Methods Appl. 1997; 30: 4607–4618.
14. Zhu L, Pan M. Hyperchaotic Oscillation and Multistability in a Fourth Order Smooth Chua System with Implementation Using No Analog Multipliers. Int. J. Bifurcat. Chaos. 2022; 32: 2250185.
15. Rajni BG. Multistability, chaos and mean population density in a discrete-time predator-prey system. Chaos, Solitons Fractals. 2022; 162: 112497.
16. Tanekou ST, Ramadoss J, Kengne J, et al. Coexistence of Periodic, Chaotic and Hyperchaotic Attractors in a System Consisting of a Duffing Oscillator Coupled to a Van der Pol Oscillator. Int. J. Bifurcat. Chaos. 2023; 33: 2330004.
17. Ahmad I, Srisuchinwong B, Jamil MU. Coexistence of Hidden Attractors in the Smooth Cubic Chua's Circuit with Two Stable Equilibria. Int. J. Bifurcat. Chaos. 2023; 33: 2330010.
18. Sahu SR, Raw RN. Appearance of chaos and bi-stability in a fear induced delayed predator-prey system: A mathematical modeling study. Chaos, Solitons Fractals. 2023; 175: 114008.
19. Cheng H, Meng X, Hayat T, Hobiny A. Multistab ility and bifurcation analysis for a three-strategy game system with public goods feedback and discrete delays. Chaos, Solitons Fractals. 2023; 175: 114011.
20. Nazmul SK, Mondal B, Thirthar AA, et al. Bistability and tristability in a deterministic prey–predator model: Transitions and emergent patterns in its stochastic counterpart. Chaos, Solitons Fractals. 2023; 176: 114073.
21. Zhang Y, Qiao Y, Duan L, Miao J. Multistability of almost periodic solution for Clifford-valued Cohen-Grossberg neural networks with mixed time delays. Chaos, Solitons Fractals. 2023; 176: 114100.
22. Recco AAC, Sagás JC, Rech PC. Multistability, period-adding, and fractality in a plasma oscillator. Phys. Plasmas. 2023; 30: 112301.
23. Sagás JC, Recco AAA, Rech PC. Chaos, periodicity, and multistability in a plasma oscillator forced by a non-sinusoidal wave function. Fundamental Plasma Phys. 2024; 12: 100072.